

Toward an Understanding of Foreground Emission in the BICEP2 Region

Raphael Flauger,^{1,2} J. Colin Hill,³ and David N. Spergel³

¹*Institute for Advanced Study, Einstein Drive, Princeton, NJ 08540, USA*

²*CCPP, New York University, New York, NY 10003, USA*

³*Dept. of Astrophysical Sciences, Peyton Hall, Princeton University, Princeton, NJ 08544, USA*

BICEP2 has reported the detection of a degree-scale B -mode polarization pattern in the Cosmic Microwave Background (CMB) and has interpreted the measurement as evidence for primordial gravitational waves. Motivated by the profound importance of the discovery of gravitational waves from the early Universe, we examine to what extent a combination of Galactic foregrounds and lensed E -modes could be responsible for the signal. We reanalyze the BICEP2 results and show that the 100×150 GHz and 150×150 GHz data are consistent with a cosmology with $r = 0.2$ and negligible foregrounds, but also with a cosmology with $r = 0$ and a significant dust polarization signal. We give independent estimates of the dust polarization signal in the BICEP2 region using a number of different approaches: (1) data-driven models based on *Planck* 353 GHz intensity, polarization fractions inferred from the same *Planck* data used by the BICEP2 team but corrected for CMB and CIB contributions, and polarization angles from starlight polarization data or the *Planck* sky model; (2) the same set of pre-*Planck* models used by the BICEP2 team but taking into account the higher polarization fractions observed in the CMB- and CIB-corrected map; (3) a measurement of neutral hydrogen gas column density N_{HI} in the BICEP2 region combined with an extrapolation of a relation between HI column density and dust polarization derived by *Planck*; and (4) a dust polarization map based on digitized *Planck* data, which we only use as a final cross-check. While these approaches are consistent with each other, the expected amplitude of the dust polarization power spectrum remains uncertain by about a factor of three. The lower end of the prediction leaves room for a primordial contribution, but at the higher end the dust in combination with the standard CMB lensing signal could account for the BICEP2 observations, without requiring the existence of primordial gravitational waves. By measuring the cross-correlations between the pre-*Planck* templates used in the BICEP2 analysis and between different versions of a data-based template, we emphasize that cross-correlations between models are very sensitive to noise in the polarization angles and that measured cross-correlations are likely underestimates of the contribution of foregrounds to the map. These results suggest that BICEP1 and BICEP2 data alone cannot distinguish between foregrounds and a primordial gravitational wave signal, and that future Keck Array observations at 100 GHz and *Planck* observations at higher frequencies will be crucial to determine whether the signal is of primordial origin.

I. INTRODUCTION

The BICEP2 collaboration has made the deepest map of the microwave sky and detected degree-scale B -mode polarization fluctuations in the Cosmic Microwave Background (CMB) [1, 2]. If these fluctuations are sourced by cosmological tensor modes, the implications for fundamental physics would be profound [3–9]. The signal would constitute direct evidence for quantum fluctuations in the spacetime metric. It would provide very strong additional support that a period of cosmic inflation occurred in the early Universe [3, 10–12]. The inferred amplitude of the tensor modes would provide a measurement of the Hubble rate during inflation ($H \approx 10^{14}$ GeV) [3] and evidence that the inflaton underwent a trans-Planckian excursion in field space [13]. In addition, it would have important implications for axion physics [14, 15], would essentially exclude cosmologically stable moduli with masses below 10^{14} GeV, and would motivate serious consideration of the gravitino problem. It would also place a direct bound on the graviton mass, $m_g \lesssim 3 \times 10^{-28}$ eV [16]. These implications would hold regardless of the precise value of the tensor-to-scalar ratio. The relatively large amplitude of the tensor modes implied by the BICEP2 signal ($r \approx 0.2$) would promise percent-level detections in coming years, which would be extremely valuable to distinguish between different inflationary models and reheating scenarios. It would also allow for the possibility of measuring the tensor tilt and testing the inflationary consistency condition.

However, the foreground estimates presented in the BICEP2 analysis already show that an understanding of foregrounds is critical for the cosmological interpretation. While the data imply a tensor-to-scalar ratio of $r = 0.2_{-0.05}^{+0.07}$ if foregrounds are not subtracted, one infers $r = 0.12_{-0.04}^{+0.05}$ after subtracting a level of foregrounds given by the auto-power spectrum of the “DDM2” foreground model in [1]. For the same model, the preliminary BICEP2 \times Keck Array data would indicate a tensor-to-scalar ratio as small as $r = 0.06_{-0.03}^{+0.04}$.

Motivated by the importance of a detection of primordial gravitational waves, this paper aims to make progress on the characterization of foreground emission in the region of sky observed by the BICEP2 collaboration. At 150 GHz,

polarized dust emission is expected to be the dominant polarized foreground, while polarized synchrotron emission is expected to dominate at lower frequencies.

The *WMAP* K (23 GHz) and Ka (33 GHz) band polarization maps provide useful templates for estimating the synchrotron contribution [17]. The BICEP2 analysis used the auto-spectrum of the K-band map and its cross-spectrum with the BICEP2 map to set an effective upper limit of $r_{\text{synch}} < 0.003$ on synchrotron contamination, quoting a spectral index of $\beta_{\text{synch}} = -3.3$. This may underestimate the importance of synchrotron emission, as the spectral index in the BICEP2 region is rather uncertain [18]. Ref. [17] finds $\beta_{\text{synch}} \approx -3.1$ at the lowest frequency range. Cross-correlating the *WMAP* measurements, *Planck* LFI observations, and the *Planck* HFI measurements, Ref. [19] reports a spectral index of $\beta_{\text{synch}} = -2.92 \pm 0.02$ for dust-correlated synchrotron over 39% of the sky. Using this index and extrapolating to 150 GHz implies that synchrotron would account for 10–15% of the amplitude of the signal in the map at 150 GHz, important enough to include in our analysis but almost certainly not large enough to account for the observed signal.

Dust polarization is potentially a more significant foreground. Although the BICEP2 region is low in Galactic dust emission and gas column density, the region appears to be more polarized than average. The three-year *WMAP* K-band data already revealed that the large-scale synchrotron polarization fraction in this region is $\sim 30\%$ (see *e.g.* Fig. 4 in Ref. [20]), and *Planck* has shown that the BICEP2 region overlaps the 30%, 40%, and 50% contours in an all-sky thresholded map of polarized intensity [21]. The very low dust intensity in the BICEP2 region therefore does not guarantee negligible polarized dust emission.

This paper is organized as follows. In section II, we discuss the prediction of the null hypothesis of a combination of synchrotron emission, dust emission, and lensed E -modes, and show that current BICEP1 and BICEP2 data cannot convincingly rule out the null hypothesis based on a measurement of the spectral index. Fortunately, the *Planck* satellite provides a powerful tool for studying dust polarization with its 217 and 353 GHz sky maps [22]. A detailed characterization of the dust emission in the BICEP2 region awaits the public release of the data and their analysis by the *Planck* collaboration, but we attempt to make progress toward the understanding of foregrounds in the BICEP2 region in section III by using temperature and polarization data from *WMAP*, temperature data from *Planck*, early *Planck* polarization results shown at the ESLAB meeting in April 2013¹, starlight polarization data, and new *Planck* polarization results presented in a recent series of papers [19, 22, 23]. According to our estimates, the amount of polarized dust emission is uncertain and could potentially be large enough to account for the excess B -mode power seen by BICEP2. To understand to what extent the cross-spectra presented by the BICEP2 collaboration provide convincing evidence that foregrounds are subdominant, we compute cross-spectra for a suite of ninety-six foreground models in section IV as well as the pre-*Planck* foreground models considered by BICEP2. We show that the noise in polarization angles in templates can lead to significant underestimates of the foreground contribution. Our conclusions are presented in section V.

II. TESTING THE NULL HYPOTHESIS

In this section, we assess whether the 100 and 150 GHz BICEP1 and BICEP2 data alone can discriminate between a cosmological signal and the null hypothesis of a combination of synchrotron, dust, and lensed E -modes. This question was also addressed by Mortonson and Seljak [24], who reach similar conclusions.

We define the null hypothesis as a Λ CDM cosmology with $r = 0$, polarized synchrotron with a level estimated from *WMAP* data, and polarized dust emission of unknown amplitude. For synchrotron, we measure the *WMAP* K-band polarization power spectrum on the BICEP2 patch and extrapolate to shorter wavelengths assuming a spectral index of $\beta_{\text{synch}} = -2.92$, which corresponds to the mean index over 39% of the sky recently derived by [19]. At $\ell = 46$, we find $\ell(\ell + 1)C_{\ell}^{BB}/2\pi = (4.0 \pm 2.7) \times 10^{-4} \mu\text{K}^2$ and $(8.9 \pm 6.1) \times 10^{-5} \mu\text{K}^2$ at 100 and 150 GHz, respectively, after filtering the maps using the BICEP1 transfer function [25]. We assume that the synchrotron power spectrum scales as $C_{\ell}^{BB} \propto \ell^{-2.6}$, consistent with *WMAP* measurements [26] and radio maps [27]. Based on the cross-correlation between starlight dust polarization and Galactic synchrotron directions [26], we assume that the polarized dust and synchrotron emissions are 70% correlated. Since the amplitude of the dust polarization signal is unknown, we allow it to vary and assume that the dust power spectrum scales as $C_{\ell}^{BB} \propto \ell^{-2.4}$ [21]. We find that the best-fit amplitude for the polarized dust component in the BICEP2 150 GHz data is $\ell(\ell + 1)C_{\ell}^{BB}/2\pi = 0.010 \pm 0.003 \mu\text{K}^2$ at $\ell = 46$, a value consistent with the range of estimates presented in section III. The two panels in Fig. 1 compare the best-fit foreground-only model and the best-fit gravitational wave-only model, both with lensed E -modes added, to the BICEP2 and BICEP1 \times BICEP2 data. Following the BICEP2 analysis, the fit only uses the five lowest multipole bins. We include cosmic variance errors and use a foreground-based spectrum for the fiducial model in the Hamimeche-Lewis

¹ http://www.rssd.esa.int/index.php?project=PLANCK&page=47_eslab

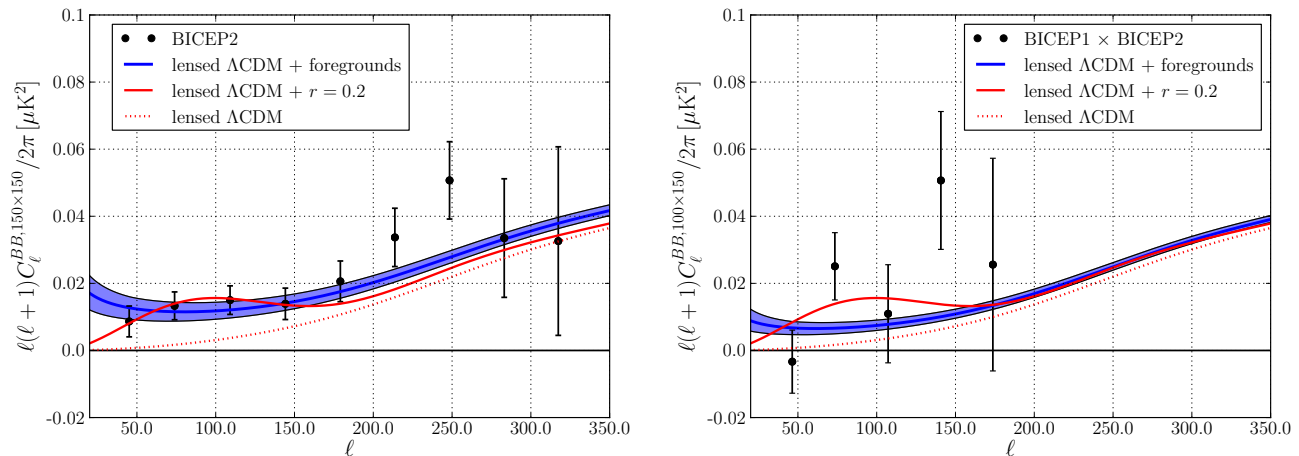


FIG. 1: The left panel compares the BICEP2 \times BICEP2 signal to two models: the best-fit lensed CMB plus gravitational wave model and the best-fit lensed CMB plus Galactic foregrounds model. The right panel compares the BICEP1 \times BICEP2 signal to the same set of models with the same parameters. The shaded band (light blue) includes uncertainties on the amplitude of the dust obtained from the BICEP2 \times BICEP2 fit, as well as uncertainties on the synchrotron amplitude and scaling with ℓ . The black error bars in both panels include sample variance for a Λ CDM cosmology with $r = 0.2$.

likelihood computation. In addition, we repeat the likelihood calculation using a Gaussian approximation and find good agreement. The null hypothesis predicts an effective spectral index $\beta \approx 1$ between 100 and 150 GHz.

Fig. 1 suggests that in the absence of a prior the foreground-only model is as good a fit to the data as the gravitational wave-only model. To quantify this, we compare simple Gaussian χ^2 values for the models for a covariance matrix that includes sample variance for a gravitational wave signal with $r = 0.2$. Using only the five lowest multipole bins of the 150×150 GHz data, we find $\chi^2 = 1.1$ for the best-fit gravitational wave-only model and $\chi^2 = 1.7$ for the best-fit foreground-only model. Using all nine multipole bins in the BICEP2 150×150 GHz power spectrum, we find $\chi^2 = 8.5$ for the best-fit gravitational wave-only model and $\chi^2 = 7.2$ for the best-fit foreground-only model. Thus, in the absence of a prior on the dust contribution, the gravitational wave-only model and the foreground-only model fit the 150 GHz data equally well.

Next, we compute the joint likelihood² of the 100×150 GHz BICEP1 \times BICEP2 data and 150×150 GHz BICEP2 data as a function of the spectral index of the signal. Following the same procedure as used in [1], we parameterize the theory input in terms of five bandpowers at 150×150 GHz and the spectral index in antenna temperature β , and marginalize over the five bandpowers. Note that the analysis in [1] also includes the 100×100 GHz BICEP1 data, which is not publicly available. Our reproduction of the analysis done in [1] is shown in red in Fig. 2. The good agreement with the constraint on the spectral index derived in [1] shows that the 100×100 GHz BICEP1 data does not significantly impact the constraints on the spectral index. We also show the results of two modified analyses: (1) we account for the contribution of the lensed E -mode signal (blue); and (2) we use cosmic variance error bars of the Λ CDM model as well as a dust contribution that fits the 150×150 GHz data (green), rather than an $r = 0$ Λ CDM model with no foregrounds. The green curve also accounts for the lensed E -mode contribution. Finally, we indicate the spectral index predicted for a model with 70%-correlated polarized synchrotron and dust emissions in orange. The final likelihood function (green posterior) is broad enough that the contribution to the signal not due to lensing is consistent with either Galactic foregrounds or gravitational waves. This is confirmed by a combined fit to the first five bandpowers of both the 100×150 GHz BICEP1 \times BICEP2 and 150×150 GHz BICEP2 data. We find $\chi^2 = 8.2$ for the best-fit gravitational wave-only model and $\chi^2 = 9.9$ for the best-fit foreground-only model. The slightly better fit for the gravitational wave-only scenario is entirely driven by the $\ell = 73$ bandpower in the 100×150 GHz BICEP1 \times BICEP2 data.

We conclude that the current BICEP1 and BICEP2 data cannot distinguish between the $r = 0.2$ model and the null hypothesis based on a spectral analysis. However, the upcoming 100 GHz data from the Keck Array could potentially strongly prefer one of these options. The null hypothesis ($r = 0$ plus foregrounds) predicts that at 100×100 GHz

² Our covariance matrix includes cosmic variance both in the diagonal and off-diagonal blocks to account for correlations between the 100×150 GHz and 150×150 GHz data.

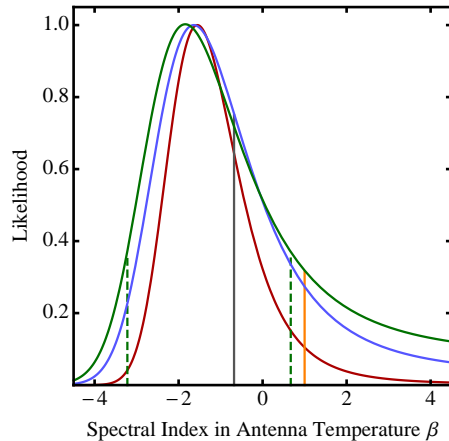


FIG. 2: Likelihood of the spectral index of the signal in antenna temperature given the 100×150 GHz BICEP1 \times BICEP2 and 150×150 GHz BICEP2 data. Because our analysis accounts for CMB lensing and includes cosmic variance errors, the likelihood function is broader than that computed in [1]. The red curve uses the same assumptions as the BICEP2 analysis and lies very close to their published result. The blue curve uses a form of the likelihood function corrected to account for CMB lensing. The green curve accounts for lensing and includes cosmic variance associated with a foreground characterized by an angular power spectrum with $\ell(\ell+1)C_\ell^{BB}/2\pi = 0.01 \mu\text{K}^2$ at $\ell = 46$, ℓ -dependence consistent with dust, and spectral index β . The covariance matrix accounts for the correlations between the 100×150 GHz and 150×150 GHz data. The vertical lines in the plot denote the best-fit CMB prediction (black) and the best-fit foreground prediction (orange). The dashed line shows the 68% confidence interval. The null-hypothesis is not convincingly excluded, but a CMB spectrum provides a better fit. However, the constraint on the spectral index is entirely driven by the second bandpower at 100×150 GHz.

$\ell(\ell+1)C_\ell^{BB}/2\pi$ at $\ell = 100$ should be $< 0.01 \mu\text{K}^2$ even under conservative assumptions about synchrotron and dust, while if $r = 0.2$, the amplitude of the signal should be significantly larger, $\sim 0.015 \mu\text{K}^2$ (in the absence of any foreground emission). Moreover, the uncertainties in the synchrotron amplitude on these scales can be reduced through cross-correlations between the *WMAP* K-band data and the Keck 100 GHz data. Thus, the Keck 100 GHz measurements may help clarify the nature of the fluctuations seen by BICEP2 at 150 GHz.

III. ESTIMATING THE DUST POLARIZATION SIGNAL

The BICEP2 team used the auto-correlations of several dust model templates as well as the cross-correlations of these templates with their data to model the polarized dust emission in the BICEP2 region and to conclude that the polarized dust contribution is negligible compared to the measured C_ℓ^{BB} , except perhaps in the lowest ℓ -bin. The analysis is based on six dust models: four of the templates referred to as FDS, BSS, LSA, and PSM are based on pre-*Planck* data, while the remaining two, DDM1 and DDM2, are driven by polarization information presented at the April 2013 ESLAB meeting. We start with a brief description of these models.

DDM1 uses the *Planck* map of Galactic thermal dust emission, which is obtained from fitting *Planck* 353, 545, and 857 GHz data, as well as IRAS 100 μm data [28]. This map is constructed at 353 GHz and then scaled to 150 GHz using a modified blackbody SED with constant emissivity 1.6 and constant temperature 19.6 K. The amplitude of polarized dust emission is then set by assuming a uniform 5% dust polarization fraction over the BICEP2 field, and Q and U maps are finally derived using polarization angles from the Planck Sky Model (PSM) [29]. PSM predictions are currently not based on *Planck* data, but rather rely on modeling informed by earlier experiments.

DDM2 uses the same dust intensity map as DDM1, but relies on a digitization of the polarization fraction and polarization angle maps presented in [30] to construct Q and U maps.

Since DDM1 does not include fluctuations in the polarization fraction, it is expected to under-predict the dust contribution to the power spectrum. For DDM2, noise bias and noise in the polarization fraction map will bias its prediction high.

The BICEP2 analysis of DDM1 and DDM2 shows polarized dust emission to be subdominant. However, this conclusion rests on a crucial input, the dust polarization fraction p in the BICEP2 field, which enters quadratically in the dust polarization auto-spectra.

The polarization fraction is also an important parameter for the remaining four models presented in [1], and was not well constrained when these models were made. A study dedicated to an understanding of the role of foregrounds

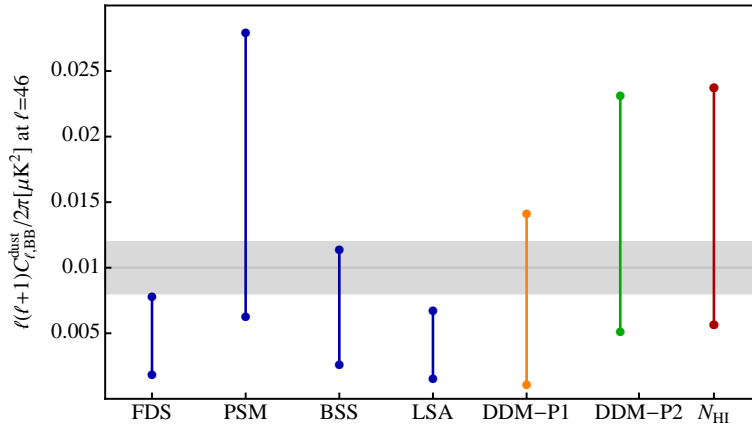


FIG. 3: Predicted contribution of polarized dust emission to the B -mode angular power spectrum for our models discussed in section III, and for the pre-*Planck* models studied by BICEP2 (blue) after taking into account the increase in polarization fraction. The range for the FDS, PSM, BSS, and LSA models, shown in blue, is based on a variation of the polarization fraction between 8 and 17%, while the range for the DDM-P1 and DDM-P2 models is based on our set of 96 models (see section III). The range for the HI estimate reflects the uncertainty in the extrapolation to low column densities and the uncertainty in frequency extrapolation. The gray band shows the best-fit amplitude of $0.010 \pm 0.002 \mu\text{K}^2$ at $\ell = 46$ determined in section II. If the dust foreground amplitude lies in this gray band, then the best-fit model to the data will have a negligible gravitational wave contribution.

for a potential future space mission (CMBPol) estimates an uncertainty of one order of magnitude for the polarization fraction [31] and hence as much as two orders of magnitude in the power spectrum. For the FDS model (based on Model 8 in [32]), the BICEP2 analysis assumes an average polarization fraction in the patch of 5%, in agreement with the average we obtain from the map shown in [30], and sets the Stokes Q and U parameters equal so that $C_\ell^{BB} = C_\ell^{EE}$. The polarization maps for the BSS and LSA models are also constructed from Model 8 in [32], with polarization fraction and angles determined from magnetic field models and line-of-sight integrals. The magnetic field model for the BSS model is a bi-symmetric spiral, and for LSA a logarithmic spiral arm. The polarization fraction is normalized to 3.6% within the *WMAP* P06 mask for both models. This yields an average polarization fraction of 5.7% and 4.9% in the BICEP2 region for the BSS and LSA models, respectively, again close to the polarization fraction obtained from [30]. Finally, for the PSM model (based on Model 7 in [32]) we find an average polarization fraction in the BICEP2 region of 5.5%.³ If the true polarization fraction were different, all these models would have to be rescaled. In other words, while only DDM1 and DDM2 explicitly rely on [30], the other four models implicitly depend on it as well.

The polarization fraction map in [30] comes with the important caveat that emission from the Cosmic Infrared Background (CIB) has not been subtracted. Based on section 2.4 of [22], the CMB may also not have been subtracted, but this potential correction is small enough to be negligible ($\sim 10\%$). As a result, the polarization fraction $p_{\text{Gal-B2}} = \sqrt{Q_{353}^2 + U_{353}^2}/I_{353}$ assumed by BICEP2 is an underestimate of the Galactic dust polarization fraction $p_{\text{Gal-Actual}} = \sqrt{Q_{\text{Gal}}^2 + U_{\text{Gal}}^2}/I_{\text{Gal}}$, where I_{Gal} is the Galactic dust intensity, I_{CIB} is the CIB intensity, I_{CMB} is the CMB intensity, and Q_{Gal} and U_{Gal} are the Galactic dust Stokes parameters, all at 353 GHz. Thus, the Galactic polarization fraction

³ We run version 1.7.8 of the PSM with the same settings as BICEP to facilitate comparison, *i.e.* run as ‘prediction’, with magnetic field pitch angle of -30° and 15% intrinsic polarization fraction. This mode misses some information about scales smaller than 3 degrees and will underpredict the degree-scale power spectrum. Simulated small scale structure is added when run in ‘simulation’ mode.

assumed in [1] is an underestimate of the true Galactic polarization fraction:

$$\begin{aligned}
 p_{\text{Gal-B2}} &= \frac{\sqrt{Q_{353}^2 + U_{353}^2}}{I_{353}} \\
 &\approx \frac{\sqrt{Q_{\text{Gal}}^2 + U_{\text{Gal}}^2}}{I_{\text{Gal}} + I_{\text{CIB}} + I_{\text{CMB}}} \\
 &= \frac{I_{\text{Gal}}}{I_{\text{Gal}} + I_{\text{CIB}} + I_{\text{CMB}}} p_{\text{Gal-Actual}}, \tag{1}
 \end{aligned}$$

Going from the first to the second line in Eq. (1) assumes that the CMB polarization level is negligible compared to the dust polarization amplitude at 353 GHz [22], and that the CIB is essentially unpolarized. Because the CIB originates from a large number of galaxies with random polarization orientations, the latter is a good approximation. Eq. (1) should be interpreted as a function of position on the sky \hat{n} , and can immediately be inverted to construct a map of the dust polarization fraction $p_{\text{Gal}}(\hat{n})$ from [30].

The polarization fraction presented in [30] was not intended for quantitative analysis, and there are significant uncertainties in its interpretation. One important uncertainty is whether the intensity map in the denominator contained a CIB monopole. Visual comparison of the recently published polarization fraction map in [22] (their Fig. 4) to that in [30] shows higher polarization fractions in [22] than in [30]. This suggests that a CIB monopole was present in the original map used by BICEP2. Removing the CIB monopole significantly increases the derived polarization fraction above the levels assumed in all of the BICEP2 models. After applying a CIB correction according to (1) to [30], we find an average dust polarization fraction of 16%, more than a factor of 3 greater than in the uncorrected map.

As a ratio of maps, the polarization fraction map depends on the zero-levels of intensity and polarization maps. Especially in regions of low emission, the uncertainties in these zero-levels translate into significant uncertainties on the polarization fraction. Marginalization over the zero levels in [30] suggests a polarization fraction of $11_{-2}^{+6}\%$ with a minimum of 8% and a long tail toward high values. These maps are very preliminary and before the release of the *Planck* polarization data a detailed analysis can only be done by the *Planck* collaboration. However, both estimates support polarization fractions a factor 2 – 3 larger than those assumed by BICEP2, indicating that the emission from dust in the region is highly polarized. This is consistent with the high polarization fractions seen in synchrotron emission in this region of the sky and is well within the range of polarization fractions seen at high Galactic latitude [22].

While the average polarization fraction is a good indicator of how large polarized foregrounds are expected to be, it is conceivable that the polarized emission is significantly stronger on large scales than on smaller scales.

All estimates of the dust polarization power spectrum based on auto-correlations scale as the square of the polarization fraction. Motivated by refs. [30] and [33], we consider a range of 8 – 17%, which leads to an increase of all estimates in [1], including those based on pre-*Planck* templates, by at least a factor 2.5 and as much as an order of magnitude. The revised estimates are shown in Figure 3. For the pre-*Planck* models, the blue bands in the plot reflect the uncertainty in the polarization fraction arising from its sensitivity to zero-levels in the polarization and intensity maps. We see that the contribution of the dust polarization according to the models is comparable to or perhaps even larger than both the BICEP2 data and the best-fit amplitude of $0.010 \pm 0.002 \mu\text{K}^2$ at $\ell = 46$ estimated in section II, which is shown as the gray band. Thus, a more detailed investigation is necessary, and we present ours in what follows.

A. Revised Data-Driven Models

Using the CIB-corrected polarization fraction map, we construct our own 150 GHz data-driven dust models (DDM-P1 and DDM-P2) and compute their auto-correlations. We scale the 353 GHz intensity map to 150 GHz using the scaling recently reported in [19], and assume that the polarization fraction does not change significantly between these two frequencies. Although [19] reports a decrease in the polarization fraction at 150 GHz relative to 353 GHz, this effect is small and does not affect our conclusions. DDM-P1 uses the average polarization fraction across the region, while DDM-P2 uses the spatially varying polarization fraction from the CIB-corrected map. Since it ignores polarization fraction fluctuations, DDM-P1 should under-predict the dust polarization levels, while noise bias and noise in the polarization fraction map will lead DDM-P2 to over-predict them.

For both DDM-P1 and DDM-P2 we consider models with different estimates for the polarization angles. Interstellar dust grains preferentially absorb the optical light from stars in the direction perpendicular to the Galactic magnetic field. As a result, their emission is polarized in this same direction, *i.e.* perpendicular to the starlight polarization direction [34]. We gathered data in the BICEP2 region from the Heiles, Santos, and Schröder samples [35–37]. Since

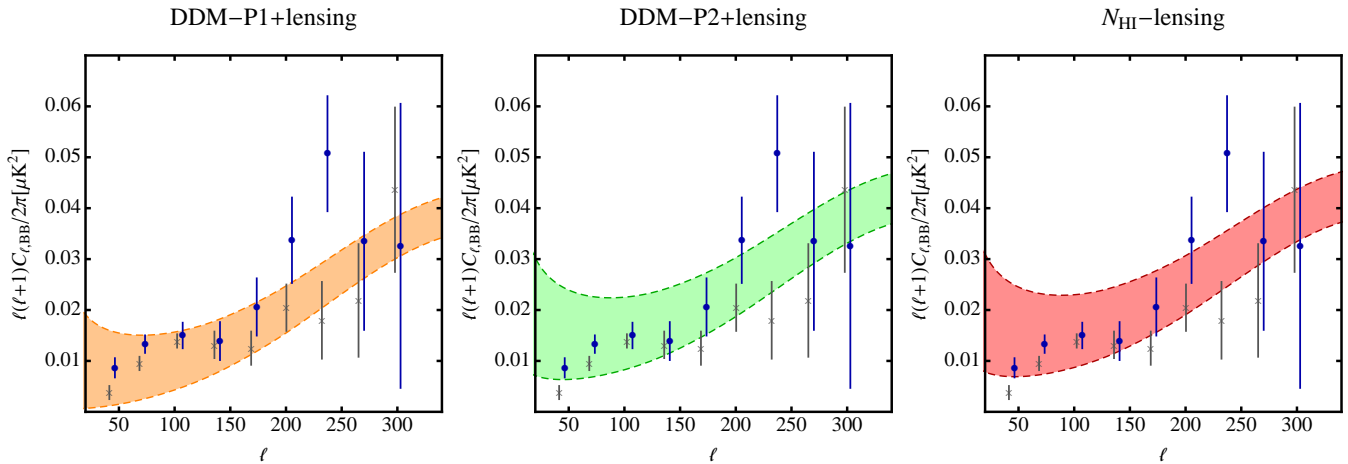


FIG. 4: Comparison of several predictions for the 150 GHz signal versus the reported BICEP2 \times BICEP2 and the preliminary BICEP2 \times Keck measurements. The predictions are a combination of the dust polarization signal and the predicted lensing signal for standard cosmological parameters. Panel (a) is based on DDM-P1, which assumes that the dust polarization signal is proportional to the dust intensity (extrapolated from 353 GHz) times the mean polarization fraction (based on our CIB-corrected map; see section III). The band represents the 1σ contours derived from a set of 48 DDM-P1 models. Panel (b) shows DDM-P2, with polarization fractions from our CIB-corrected map, and polarization direction based on starlight measurements, the PSM, or [33]. Panel (c) uses the column density of neutral hydrogen in the BICEP2 region inferred from the optical depth at 353 GHz to estimate the dust foreground. In this panel, the band reflects the uncertainty in the extrapolation of the scaling relation to low column densities as well as the uncertainty in the rescaling from 353 GHz to 150 GHz.

this region has been selected by the BICEP2 team for its low dust extinction, few starlight polarization data have been collected within the field. However, we found seven significant detections ($P/\sigma_P > 1$) along sightlines to stars at least 100 pc above the Galactic plane. Two of them are for the same star, but observed by different teams, with both observations above 5σ . The polarization angle of the dust emission derived from the latter is 154.5° . The mean and median angles derived from all significant detections in the region are respectively 171.1° and 160.4° , in good agreement with that derived from the 5σ detections. In a first class of models, we thus take the polarization angle to be constant across the patch, and explore a range of values consistent with starlight polarization data, taking the average dust emission polarization angle to be 160° , and explore the effect of varying this angle by 10° .

In a second class of models, we again take the polarization angle to be constant across the patch, but use the average polarization angle from the PSM. We consider a third class of models, in which we use polarization angles derived from the PSM after smoothing the maps to 1 or 5 degrees. Finally, we consider models based on [33] and vary the zero levels of the polarization and intensity maps within errors of the calibration.

The first two panels of Fig. 4 show the range of dust B -mode amplitudes compatible with each model added to the lensed E -mode signal. The DDM-P1/DDM-P2 envelopes correspond to the 1σ contours based on a suite of forty-eight DDM-P1/DDM-P2 models that differ by their choice of polarization angles and map zero-levels, as discussed above. DDM-P1 and DDM-P2 lead to consistent predictions, and the uncertainty envelope on each estimate encompasses the BICEP2 and BICEP2 \times Keck data points in the five bins used in the BICEP2 analysis.

B. Estimate from HI Column Density

The *Planck* collaboration has reported a strong correlation between HI column density and the amplitude of the dust polarization signal along a given line of sight [21]. We use this relationship to estimate the polarization signal in the BICEP2 region. HI column density can be inferred from the *Planck* 353 GHz dust opacity map according to $N_{\text{HI}} = 1.41 \times 10^{26} \text{ cm}^{-2} \tau_{353}$ [28]. Using this relation, we find $N_{\text{HI}} = (1.50 \pm 0.07) \times 10^{20} \text{ cm}^{-2}$ in the BICEP2 region.⁴ Inserting this value into the relation between N_{HI} and dust polarization amplitude and using the appropriate modified blackbody SED [19], at 150 GHz we obtain polarized dust emission power estimates at $\ell = 100$ of $0.021 \pm 0.014 \mu\text{K}^2$ for $\ell(\ell+1)C_\ell^{EE}/2\pi$ and $0.015 \pm 0.010 \mu\text{K}^2$ for $\ell(\ell+1)C_\ell^{BB}/2\pi$.

⁴ While Ref. [21] was based on an older version of the *Planck* dust model, we consistently work with version 1.20.

The third panel in Fig. 4 shows the predicted range of the polarized Galactic dust emission inferred from the above procedure combined with the lensed CMB signal. The primary caveats of this method are that it involves applying scaling relations calibrated for large sky fractions and high HI column densities to the BICEP2 region, which covers only $\sim 1\%$ of the sky and has a low HI column density, and that it assumes that the same scaling relations hold at 353 GHz and 150 GHz. In addition, the scatter in the relations is likely to increase as one proceeds to smaller HI column densities similar to those in the BICEP2 region. With these caveats in mind, we note the good agreement between the HI estimate and those relying on the DDM-P1 and DMM-P2 models shown in the leftmost panels of Fig. 4. This suggests that although each of the methods used to derive the estimates shown in Fig. 4 comes with its own caveats, the prediction of a high level of 150 GHz polarized dust emission in the BICEP2 field is robust.

C. Consistency Check

We compare our estimates for the dust polarization signal in the BICEP2 region to a measurement of the angular power spectrum from the maps presented in [33] in the BICEP2 region. To understand the properties of these maps, we have reproduced the analyses in [21] and find good agreement. Furthermore, we have computed cross-spectra with the *WMAP* W-band data and find good agreement with the 100×353 GHz spectra presented in [21]. Additional cross-correlations with lower frequency *WMAP* data provide further evidence that the maps are reliable, making a measurement of their power spectrum worthwhile. We stress that none of the conclusions in this paper rely on digitizing the maps in [33]. However, this exercise constitutes a useful cross-check of the work already presented, and also allows us to demonstrate the internal consistency of the results presented by *Planck* in [21, 30, 33].

Our power spectrum estimator is based on PolSpice [38]. We have carefully set the PolSpice parameters to ensure that we recover the input angular power spectra on the BICEP2 patch using 250 CMB-only simulations, filtered with the BICEP1 filter function. Our filtering is isotropic, while that of BICEP2 is not. However, given the high degree of isotropy of the filtered dust maps we do not expect this to alter the conclusions.

The maps contain two sources of noise that are a priori unknown: the noise of the instrument, and the noise introduced by the digitization. For the instrumental noise, we assume that its shape is well described by the *Planck* noise model with parameters identical to those for intensity. To understand the noise introduced by digitization, we have developed a pipeline that takes HEALPix maps, converts them to GIF files, and inserts them into a presentation which is then saved as a PDF file. We then apply our digitization procedure to convert the PDF files back to GIFs and then to HEALPix data files. At 353 GHz, the polarized emission is dominated by dust. We thus apply this pipeline to ten simulations of dust maps. This has allowed us to characterize the effects introduced by the digitization procedure in the form of a transfer function. In addition to the dust, the maps contain instrument noise. We thus process ten noise simulations through our pipeline and measure the corresponding transfer function. We assume that the power spectrum of the map is well described by $C_\ell^{\text{obs}} = F_\ell^{\text{Dust}} C_\ell^{\text{Dust}} + A F_\ell^{\text{Noise}} N_\ell$, where F_ℓ are the transfer functions measured in the simulations, C_ℓ^{Dust} is the underlying dust power spectrum, N_ℓ is the *Planck* noise model with parameters extracted from a fit to the half-ring half-difference for the 353 GHz intensity maps, and A is a fitted amplitude.

We can extrapolate our measurement at 353 GHz to 150 GHz using the dust properties from [19] as before to predict the dust polarization signal. The resulting level is consistent with the predictions from the previous methods shown in Fig. 4. Given that the maps in [30] have not yet been released by *Planck*, we choose not to show the derived spectrum next to those in Fig. 4 as an acknowledgment of the preliminary nature of these maps. We only consider them here as a final cross-check, as even in their preliminary form, they represent the best publicly available maps of dust polarization, as well as a significant improvement over our pre-*Planck* knowledge of foregrounds.

IV. CROSS-CORRELATION ESTIMATES FROM POLARIZATION TEMPLATES

Cross-correlations with templates that very accurately trace the foreground polarization can provide a precise estimate of the contribution of the foreground to a map. However, this requires that there be little noise in the foreground template and that it correctly capture the spatial structure of the actual foreground. If the foreground template differs in spatial structure from the actual foreground, then any measurement of the cross-correlation will underestimate the contribution of the foreground to the power spectrum.

Since the BICEP2 maps are not publicly available, we cannot directly test cross-correlations with these maps. However, we can test the templates by measuring their cross-correlations. If the cross-correlations between the templates are significantly below 1 (as shown in Figure 5), then negligible correlations between data and these templates do not imply that foregrounds are negligible.

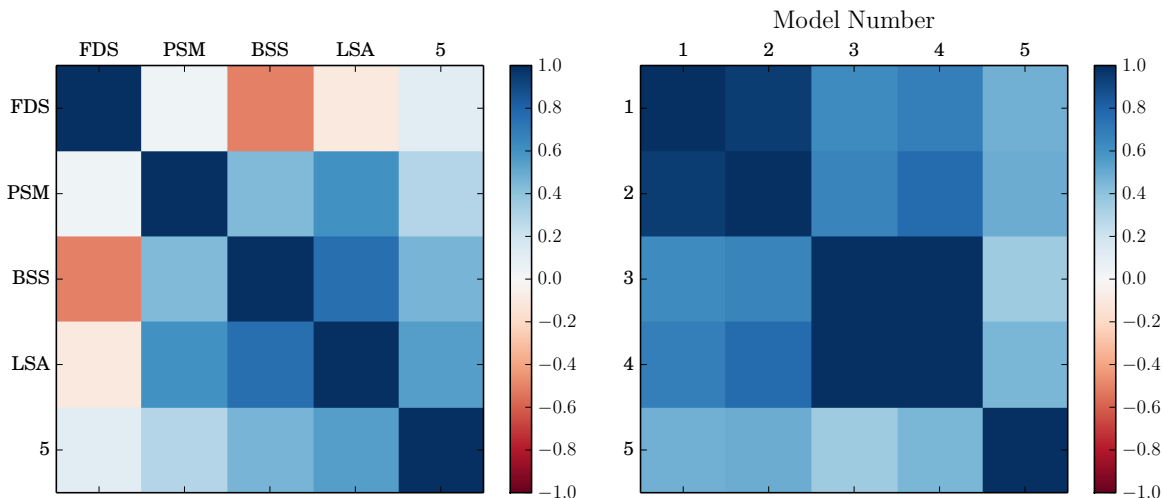


FIG. 5: The left panel shows the correlation matrix at $\ell = 46$ for model 5 and four of the templates used in [1]: the Planck Sky Model (PSM) [29], the Bi-Symmetric Spiral (BSS) and Logarithmic Spiral Arm (LSA) field models presented in [39], and Model 8 of [32] with $Q = U$. If the true sky looked like one of the models, then a measurement of the cross-correlation using another model would underestimate the signal by as much as a factor of 10. The correlations further decrease for higher multipoles. The right panel shows the correlation matrix at $\ell = 46$ for a small subset of five DDM-P2 dust models. The polarization angles are taken to be (1) the average angle in the patch as inferred from starlight data; (2) the average angle taken from the PSM; (3) from the PSM at 5 degree resolution; and (4) from the PSM at 1 degree resolution. Model 5 is based on [33] and is a proxy for data. Even between “data-based” models and data, correlation coefficients below 50% are common, suggesting that low cross-power between the data-driven models and data do not establish that foregrounds are negligible.

As discussed in section III, Ref. [1] used a series of templates that are based on multiplying the intensity of the dust signal by a polarization fraction and a polarization direction. While the publicly available *Planck* 353 GHz maps and dust models provide an accurate map of the dust intensity signal, the polarization directions and the polarization amplitudes are poorly known. We can estimate the sensitivity of the measured cross-correlations to the polarization angle by cross-correlating the four publicly available templates used in [1] with themselves and the maps from [33], which we will refer to as model 5 below. The matrix of correlation coefficients at $\ell = 46$ is shown in the left panel of Figure 5. The small correlations between the templates and between the templates and model 5 suggest that the small cross-correlations with the data measured in [1] likely reflect the limitations of the templates and do not provide a constraint on the dust polarization.

As a test for the revised data-driven models, we have computed the full set of cross-spectra for our suite of ninety-six models (see section III A). For clarity, we focus the discussion on a small representative subset of five DDM-P2 models selected to illustrate the main conclusions from our analysis. In all five DDM-P2 models shown, the dust polarization fraction is set from our CIB-corrected map (see section III). We then set polarization angles in one of five ways: model 1 assumes a constant polarization angle set from starlight polarization data (see section III A); model 2 assumes a constant polarization angle set from the Planck sky model; models 3 and 4 use spatially-varying polarization angles again set from PSM maps, but smoothed to 5° and 1° , respectively, before computation of the polarization angles; and model 5 is based on the maps discussed in section III C.

The correlation matrix for these models at $\ell = 46$, corrected for noise bias, is shown in the right panel of Fig. 5. The two models with constant polarization angles (models 1 and 2) correlate well with each other, which is expected since the polarization angles obtained from starlight data and from the PSM are in good agreement. Similarly, the models whose polarization angles are based on the smoothed PSM maps (models 3 and 4) also correlate well with each other, and the correlations between these models and the first two are still significant. However, the correlations between model 5, our proxy for data, and any other model are typically suppressed by a factor of two to three. Such a suppression is quite typical in our full 96×96 correlation matrix, and in fact much lower correlation coefficients and even small negative ones exist. The correlation coefficients decrease further on smaller scales.

Model 5 is the only model whose polarization angles are set from polarized dust emission data. Although preliminary, as discussed in section III C, these data are the only of their kind currently publicly available. The suppressed correlation between model 5 and the other models, and more generally between models with polarization angles set

from data and other models, therefore suggests that the cross-spectra between the six templates studied by BICEP2 and their data could significantly underestimate the true foreground level in their field. Uncertainties in the spatial variation of the polarization fraction, turbulence-driven variations in the polarization direction, and noise in the maps used to generate the template will further suppress the cross-correlation and lead to even more severe underestimates. We note that these effects are even larger on smaller scales and may explain the trends seen in the cross-correlation between DDM2 and the BICEP2 150 GHz data shown in Fig. 6 of [1].

The *Planck* 217 and 353 GHz data should provide an excellent template for cross-correlation analysis. Ref. [19] showed that the polarized dust emission at 150 GHz is expected to be highly (but not perfectly) correlated with dust at higher frequencies and the noise properties of these maps (when released) should be well characterized. From the public intensity maps we already know that, because of the *Planck* scan strategy, the noise levels in the maps in the BICEP2 region of the sky are about 80% of the average.

In conclusion, cross-spectra with templates that are not based directly on observed dust polarization data cannot convincingly establish that foregrounds in the BICEP2 region are truly negligible. This uncertainty will be significantly reduced when the BICEP2 150 GHz maps can be directly cross-correlated with the *Planck* 217 and 353 GHz polarization data.

V. CONCLUSION AND OUTLOOK

Motivated by the importance of the detection of gravitational waves for our understanding of cosmology, we have examined the uncertainties in the amplitude of the dust polarization signal in the BICEP2 region. We conclude that the predicted level of polarized emission from interstellar dust in this field might leave room for a primordial gravitational wave contribution, but could also be high enough to explain the observed excess B-mode power. Thus, no strong cosmological inference can be drawn at this time.

We are in the fortunate situation that the Keck Array 100 GHz maps, the *WMAP* K-band and *Planck* LFI maps, the *Planck* HFI polarization maps, and the BICEP2 150 GHz maps will soon help us determine the relative contributions of dust, synchrotron, and the CMB to the signal detected by BICEP2, and may then lead to a definitive discovery of gravitational waves.

Acknowledgments

We thank Steve Choi, Renée Hložek, William Jones, Lyman Page, Uros Seljak, Suzanne Staggs, Paul Steinhardt, and Matias Zaldarriaga for stimulating conversations, Andrei Berdyugin for pointing us to the Schröder and Santos starlight polarization catalogs, and in particular Aurélien Fraisse for his numerous contributions to the paper.

RF gratefully acknowledges the Raymond and Beverly Sackler Foundation for their support. RF is also supported in part by NSF grants PHY-1213563 and PHY-0645435. JCH and DNS are supported by NASA Theory Grant NNX12AG72G and NSF AST-1311756.

-
- [1] BICEP2 Collaboration, Ade, P. A. R., Aikin, R. W., et al. 2014, arXiv:1403.3985
 - [2] BICEP2 Collaboration, Ade, P. A. R., Aikin, R. W., et al. 2014, arXiv:1403.4302
 - [3] A. A. Starobinsky, JETP Lett. **30**, 682 (1979) [Pisma Zh. Eksp. Teor. Fiz. **30**, 719 (1979)].
 - [4] A. G. Polnarev, 1985, Sov. Ast., 29, 607
 - [5] Davis, R.L., Hodges, H.M., Smoot, G.F., Steinhardt, P.J., & Turner, M., 1992 Physical Review Letters, 69, 1856.
 - [6] Crittenden, R., Bond, J.R., Davis, R.L., Efstathiou, G. & Steinhardt, P.J. 1993, Physical Review Letters, 71, 324.
 - [7] Seljak, U. 1997, Astrophys. J., 482, 6
 - [8] Seljak, U., & Zaldarriaga, M. 1997, Physical Review Letters, 78, 2054
 - [9] Kamionkowski, M., Kosowsky, A., & Stebbins, A. 1997, Physical Review Letters, 78, 2058
 - [10] Guth, A. H. 1981, Phys. Rev. D, 23, 347
 - [11] Linde, A. D. 1982, Physics Letters B, 108, 389
 - [12] Albrecht, A., & Steinhardt, P. J. 1982, Physical Review Letters, 48, 1220
 - [13] Lyth, D. H. 1997, Physical Review Letters, 78, 1861
 - [14] P. Fox, A. Pierce and S. D. Thomas, hep-th/0409059
 - [15] D. J. E. Marsh, D. Grin, R. Hložek and P. G. Ferreira, arXiv:1403.4216 [astro-ph.CO].
 - [16] S. Dubovsky, R. Flauger, A. Starobinsky and I. Tkachev 2010, Phys. Rev. D, 81, 023523 [arXiv:0907.1658 [astro-ph.CO]]
 - [17] Bennett, C. L., Larson, D., Weiland, J. L., et al. 2013, Astrophys. J. Supp., 208, 20
 - [18] Fuskeland, U., Wehus, I. K., Eriksen, H. K., & Næss, S. K. 2014, arXiv:1404.5323

- [19] Planck Collaboration Int. XXII. 2014, A&A, submitted [arXiv:1405.0874]
- [20] A. Kogut et al. 2007, *Astrophys. J.*, 665, 355 [arXiv:0704.3991 [astro-ph]]
- [21] rssd.esa.int/SA/PLANCK/docs/eslab47/Session09_Data_Processing/47ESLAB_April_04_10_30_Aumont.pdf
- [22] Planck Collaboration Int. XIX. 2014, A&A, submitted [arXiv:1405.0871]
- [23] Planck Collaboration Int. XXI. 2014, A&A, submitted [arXiv:1405.0873]
- [24] Mortonson, M.J. & Seljak, U. 2014, arXiv:1405.5857
- [25] Barkats, D., Aikin, R., Bischoff, C., et al. 2014, *Astrophys. J.*, 783, 67
- [26] Page, L. et al. 2007, *Astrophys. J., Suppl. Ser.*, 170, 335
- [27] La Porta, L., Burigana, C., Reich, W., & Reich, P. 2008, *Astron. Astrophys.*, 479, 641
- [28] Planck Collaboration XI. 2014, A&A, submitted [arXiv:1312.1300]
- [29] Delabrouille, J., Betoule, M., Melin, J.-B., et al. 2013, *Astron. Astrophys.*, 553, A96
- [30] rssd.esa.int/SA/PLANCK/docs/eslab47/Session07_Galactic_Science/47ESLAB_April_04_11_25_Bernard.pdf
- [31] Dunkley, J., Amblard, A., Baccigalupi, C., et al. 2009, *American Institute of Physics Conference Series*, 1141, 222
- [32] Finkbeiner, D.P., Davis, M. & Schlegel, D.J. 1999, *Astrophys. J.*, 524, 867
- [33] rssd.esa.int/SA/PLANCK/docs/eslab47/Session04_Astrophysical_Results/47ESLAB_April_03_14_50_Boulanger.pdf
- [34] Draine, B. T., *Physics of the Interstellar and Intergalactic Medium*. Princeton University Press, 2011
- [35] Heiles, C. 2000, *Astron. J.*, 119, 923
- [36] Santos, F. P., Corradi, W., & Reis, W. 2011, *Astrophys. J.*, 728, 104
- [37] Schröder, R. 1976, *Astron. Astrophys. Supp.*, 23, 125
- [38] Chon, G., Challinor, A., Prunet, S., Hivon, E., & Szapudi, I. 2004, *Mon. Not. R. Astron. Soc.*, 350, 914
- [39] O’Dea, D.T., Clark, C.N., Contaldi, C.R., & MacTavish, C.J. 2012, *Mon. Not. R. Astron. Soc.*, 419, 1795